Data-driven Estimation for a Region of Attraction for Transient Stability Using the Koopman Operator

Le Zheng, *Member*, *IEEE*, Xin Liu, Yanhui Xu, *Member*, *IEEE*, Wei Hu, *Senior Member*, *IEEE*, and Chongru Liu, *Senior Member*, *IEEE*

***Abstract*—This paper presents a novel Koopman Operator based framework to estimate the region of attraction for power system transient stability analysis. The Koopman eigenfunctions are used to numerically construct a Lyapunov function. Then the level set of the function is utilized to estimate the boundary of the region of attraction. The method provides a systematic method to construct the Lyapunov function with data sampled from the state space, which suits any power system models and is easy to use compared to traditional Lyapunov direct methods. In addition, the constructed Lyapunov function can capture the geometric properties of the region of attraction, thus providing useful information about the instability modes. The method has been verified by a simple illustrative example and three power system models, including a voltage source converter interfaced system to analyze the large signal synchronizing instability induced by the phase lock loop dynamics. The proposed method provides an alternative approach to understanding the geometric properties and estimating the boundary of the region of attraction of power systems in a data driven manner.**

***Index Terms*—Koopman operator, lyapunov function, power system transient stability, region of attraction.**

I. Introduction

TRANSIENT stability assessment is one of the most significant tasks in power systems research. In traditional power systems, transient stability is the ability of synchronous machines to remain in synchronism after being subjected to a large disturbance [1]. With significant integration of converter interfaced generation (CIG), loads, and transmission devices, the dynamic response of the power electronics dominated power systems has become more dependent on power electronic devices [2]. The increasing nonlinearity and dimensionality poses more challenges and difficulties to the development of transient stability assessment tools.

There are broadly four main techniques to analyze transient stability. One is the time domain simulation, that computes trajectories of the state variables through numerical integration of the system's ordinary differential equations (ODEs) or differential algebraic equations (DAEs) [3]. Time domain simulation is the simplest and most frequently used stability analysis method. However, numerical integration is very time consuming when the system is large, especially in power systems with high penetration of electronic devices. Time domain simulation also requires that the governing equations should have precise parameters, which is difficult in real world power system analysis.

Dr. Xue has developed the extended equal-area criterion (EEAC) and built rigorous mathematic foundations to make EEAC applicable to real world applications during the last century [4]. EEAC provides unified formulations for various system models and provides the necessary and sufficient conditions for large disturbance stability. EEAC is a good candidate for online transient stability assessment. But since EEAC is disturbance dependent, it is usually very time consuming to estimate the boundary of the ROA.

Another technique turns the transient stability assessment into a binary classification task, and uses data driven methods to determine the classification boundaries. It has become popular with the fast development of artificial intelligence [5]–[8]. It consists of two stages, the offline training stage and the online assessment stage. The computing burden has been transferred to the offline training stage, thus it is suitable for online applications. However, the learned classification boundaries by the artificial intelligence algorithms lack interpretations and physical insight, which has kept this method from practical applications.

The fourth and most classic technique is the Lyapunov direct method [9]–[13], that has solid theoretic foundations and is able to compute the region of attraction (ROA) using the level sets of the Lyapunov function (LF). The core task of the direct method is to find a LF having certain properties. However, there exists no general approaches for constructing such functions. Two commonly used construction methods include the transient energy functions (TEFs) method [9]–[11] and the polynomial optimization method, such as the sum of squares (SOS) [12], [13] and linear matrix inequalities (LMI). TEFs are only known for a small class of power system models, and the critical potential energy at the boundary of the ROA is hard to compute in large systems. The polynomial optimization method is hard to generalize in large scale systems since the computation burden increases exponentially. In addition, the SOS method cannot capture the manifold information of the unstable equilibrium points (UEP) around

Manuscript received December 20, 2021; revised March 24, 2022; accepted May 10, 2022. Date of online publication October 12, 2022; date of current version February 1, 2023. This work was supported by the National Key R&D Program of China Response-driven intelligent enhanced analysis and control for bulk power system stability (2021YFB2400800).

L. Zheng, X. Liu, Y. H. Xu, and C. R. Liu (corresponding author, email: chongru.liu@ncepu.edu.cn) are with the School of Electrical and Electronic Engineering, North China Electric Power University, Beijing 102206, China.

W. Hu is with the Department of Electrical Engineering, Tsinghua University, Beijing 100084, China.

DOI: 10.17775/CSEEJPES.2021.09360

the stable equilibrium point (SEP); thus it is unable to provide additional knowledge about the instability modes.

Therefore, it is preferred to have a LF construction tool that is suitable for any power system models and capable of parameterizing the structure of the manifold around the SEP to estimate the ROA. Over the last decade, there is a growing interest in the Koopman Operator framework in the nonlinear community. Mezic *et al* showed that the eigenfunctions of the Koopman Operator reveal important global geometric properties of the underlying nonlinear system [14]–[16]. Another attractive point of the Koopman Operator is that it is amenable to data driven analysis through the so-called Koopman mode decomposition and is directly connected to efficient numerical algorithms [17]–[20]. The Koopman Operator framework has been widely applied in the context of nonlinear control [21], [22], system identification [23], and stability analysis [24], [25]. References [26]–[30] have made pioneering efforts in utilizing the Koopman Operator for power system oscillation analysis and nonlinear transformations. Susuki *et al* showed that the Koopman mode analysis enables the decomposition of nonlinear dynamic phenomena into relevant modes and is suitable for identifying the emergent energy transmission and coherent machines during large disturbances [26], [27], but it is unable to estimate the ROA. Choi *et al* proposed to check the changes of the dominant Koopman eigenfunction magnitude and compute the boundary of ROA when detecting sharp increases [30]. However, Choi claims that the technique lacks theoretical guarantees and needs further investigation.

The main contributions of this paper are twofold. First, we introduce a data driven algorithm to estimate the ROA based on the Koopman Operator. Based on recent advances in the Koopman Operator, a data driven LF construction method using the Koopman eigenfunctions is proposed. The largest closed level set of the LF in the region where the LF is strictly decreasing along the trajectories provides an inner estimation of the ROA. Second, we improve the Koopman Operator approximation algorithm considering the nonlinear function characteristics of the power system models. Using the method presented in [30], we are able to unify the elementary nonlinear functions in most power system models, such as $\sin x$, $\cos x$, to the polynomial format, which is used to form a N-order polynomial basis function in approximating the Koopman eigenfunctions.

To the best of our knowledge, our method is the first to construct Lyapunov functions and estimate the region of attraction for power system transient stability analysis using the Koopman Operator. The rest of the paper is organized as follows: Section II provides a brief introduction of the Koopman Operator and recent advances in global stability analysis using the operator. The ROA estimation method is presented in Section III. In addition, a novel Koopman Operator approximation method considering the characteristics of power system models is designed to improve the estimation accuracy. In Section IV, an illustrative example and three power system models are used to test the proposed method. More specifically, the Single Machine Infinite Bus (SMIB) system and a voltage source converter (VSC) connected to a weak AC grid system are compared side by side to demonstrate that the proposed method is both valid for traditional generators and CIGs. The two-machine infinite bus (TMIB) system is used to show that the method is capable of identifying the geometric properties for multiple equilibrium point scenarios. A critical discussion of the method is also presented, including further extensions required to generalize this analysis to large scale and real systems. Section V concludes the main results of this study.

II. Preliminaries on Koopman Operator

The electromechanical and electromagnetical dynamics of power systems can be described by ODEs defined in the state space according to the implicit function theorem [3]. As shown in (1), f represents the ODEs, and $x \in \mathbb{R}^N$ is the N-dimension vector of dynamical state variables of the power system model, including generator rotor angles, q-axis voltage of the VSC interfaced generation, etc.

$$\dot{x} = f(\boldsymbol{x}) \tag{1}$$

The ODEs are highly nonlinear and it is difficult to analyze the stability properties directly in the state space. The Koopman Operator provides an alternative description of the dynamics in a linear but infinite dimensional observable space (see [16], [31] for a review). The linear evolution of the observables is equivalent to the nonlinear evolution of the states; thus the operator-theoretic description provides a global insight into the system dynamics which is appropriate for global linearization and stability analysis. Below we will provide a brief introduction on the Koopman Operator, as well as related theorems and various results on stability analysis.

A. Koopman Operator and Its Spectral Decomposition

Consider a space $\mathcal{G}$ of observables $g : \mathbb{R} \to \mathbb{C}$. The Koopman Operator $K : \mathcal{G} \to \mathcal{G}$ is defined as a map in the observable space associated with the dynamical system through the composition:

$$Kg = g \circ S^t \equiv g(S^t) \tag{2}$$

where $S^t = \boldsymbol{x}(0) + \int_0^t f(\boldsymbol{x}(\boldsymbol{\tau}))\mathrm{d}\boldsymbol{\tau}$ is the flow map of (1).

The Koopman Operator offers two main advantages. First, it provides a global picture of the system, without any further assumptions or approximations. Second, it provides a linear approach to analyze the nonlinear dynamics. However, the price we have to pay is that the Koopman Operator is infinitely dimensional for most cases.

Since the operator is linear, it is natural to study the operator by its spectral properties, *i.e.* eigenvalues and eigenfunctions. More importantly, finite dimensional projections onto the eigenspace can partially solve the infinite dimensionality challenge. An eigenfunction of the Koopman Operator associated with the dynamical system is an observable function $\varphi_\lambda \in \mathcal{G}\backslash\{0\}$ that satisfies:

$$K\boldsymbol{\varphi}_\lambda = \boldsymbol{\varphi}_\lambda(S^t) = e^{\lambda t}\boldsymbol{\varphi}_\lambda,\ \forall t \geq 0 \tag{3}$$

where $\lambda \in \mathbb{C}$ is the corresponding eigenvalue. There is an infinity of Koopman eigenvalue and eigenfunction pairs [16], though they can be dependent. For a hyperbolic equilibrium of a nonlinear system, the eigenvalues of the Jacobian matrix at the equilibrium are also the Koopman eigenvalues of the system, and they are called the principle eigenvalues [25], which are directly related to the stability properties.

B. Finite Dimensional Approximations

Since the Koopman Operator is infinitely dimensional, it is necessary to consider finite dimensional approximations for practical purposes. There are already lots of methods, both analytical, such as series expansions [31], and numerical, such as Dynamic Mode Decomposition (DMD) [17], Extended DMD (EDMD) [18], and Tunable Accuracy Symmetric Subspace Decomposition (T-SSD) [19], [20] etc. Among them, EDMD is the most intuitive method considering (2).

The EDMD algorithm is a data driven Koopman Operator discovery procedure and all the input data are evenly sampled from the flow map S^t. Therefore, we first discretize (1) with sampling period Δt to get the discrete form:

$$\boldsymbol{x}_{k+1} = F(\boldsymbol{x}_k) \tag{4}$$

where $\boldsymbol{x}_k = \boldsymbol{x}(k\Delta t)$. The discrete time Koopman Operator is defined as:

$$Kg = g(F) \tag{5}$$

In other words, we have:

$$Kg(\boldsymbol{x}_k) = g(F(\boldsymbol{x}_k)) = g(\boldsymbol{x}_{k+1}) \tag{6}$$

Similarly, the discrete time Koopman eigenvalue and eigenfunction have the form:

$$K\boldsymbol{\varphi}_\lambda = \lambda\boldsymbol{\varphi}_\lambda \tag{7}$$

EDMD requires two prerequisites. One is a data set of snapshot pairs sampled from the state space:

$$\boldsymbol{X} = [\boldsymbol{x}_0, \boldsymbol{x}_1, \cdots, \boldsymbol{x}_{k-1}], \quad \boldsymbol{Y} = [\boldsymbol{x}_1, \boldsymbol{x}_2, \cdots, \boldsymbol{x}_k] \tag{8}$$

where $\boldsymbol{X}, \boldsymbol{Y} \in \mathbb{R}^{N\times k}$, $\boldsymbol{x}_i$ a column vector of the state variables at the i-th time stamp. The other is a M-dimension vector of scalar functions, which is also called the basis function:

$$\Psi(\boldsymbol{x}) = [\psi_1(\boldsymbol{x}), \psi_2(\boldsymbol{x}), \cdots, \psi_{\mathrm{M}}(\boldsymbol{x})] \tag{9}$$

The basis function is used to lift the system from the N-dimension state space to the M-dimension observable space.

$$\begin{aligned}\boldsymbol{X}_{\text{lift}} &= [\Psi(\boldsymbol{x}_0), \Psi(\boldsymbol{x}_1), \cdots, \Psi(\boldsymbol{x}_{k-1})], \\ \boldsymbol{Y}_{\text{lift}} &= [\Psi(\boldsymbol{x}_1), \Psi(\boldsymbol{x}_2), \cdots, \Psi(\boldsymbol{x}_k)]\end{aligned} \tag{10}$$

where $\boldsymbol{X}_{\text{lift}}, \boldsymbol{Y}_{\text{lift}} \in \mathbb{R}^{M\times k}$. According to (6) we have $K\boldsymbol{X}_{\text{lift}} = \boldsymbol{Y}_{\text{lift}}$, so the finite dimensional approximation of the Koopman Operator in a least square sense is:

$$K = \boldsymbol{Y}_{\text{lift}}\boldsymbol{X}_{\text{lift}}^{\dagger} \tag{11}$$

where $\boldsymbol{X}^\dagger$ denotes the Moore-Penrose pseudoinverse of $\boldsymbol{X}$ and $K \in \mathbb{R}^{M\times M}$. The eigenvalues of K are approximations to the Koopman eigenvalues, and the associated eigenfunctions are:

$$\boldsymbol{\varphi}_{\lambda_j}(\boldsymbol{x}) = w_j^{\mathrm{T}}\Psi(\boldsymbol{x}) \tag{12}$$

where w_j is the left eigenvectors of K corresponding to λ_j, T denotes the transpose operator. We easily verify that:

$$\begin{aligned}(K\boldsymbol{\varphi}_{\lambda_j})(\boldsymbol{x}) &= \boldsymbol{\varphi}_{\lambda_j}(F(\boldsymbol{x})) = w_j^{\mathrm{T}}\Psi(F(\boldsymbol{x})) \\ &= w_j^{\mathrm{T}}K\Psi(\boldsymbol{x}) = \lambda_j w_j^{\mathrm{T}}\Psi(\boldsymbol{x}) = \lambda_j\boldsymbol{\varphi}_{\lambda_j}(\boldsymbol{x})\end{aligned} \tag{13}$$

Equation (11) involves Moore-Penrose pseudoinverse and matrix multiplication computation, which can be quickly solved by mature algorithms even for huge matrices. Therefore, the negative effect introduced by high dimension is limited. The accuracy and rate of convergence of EDMD is primarily dependent on the choice of the basis function. If we use the state variables, EDMD reduces to DMD. How to find proper basis functions to observe the nonlinear dynamics is still an open question.

C. Global Stability Analysis Based on the Koopman Operator

The main result used in this paper about stability analysis is described in the following theorems. More interesting conclusions are referred to in [25].

Proposition 1. Let $X \in \mathbb{R}^N$ be a connected, forward invariant, compact set. Consider (1) with $f \in C^2(X)$ admits a hyperbolic fixed point $\boldsymbol{x}^* \in X$ and assumes that the Jacobian matrix ϑ at $\boldsymbol{x}^*$ has N distinct eigenvalues with strictly negative real parts. Then, the fixed point is globally stable if and only if the Koopman Operator associated with (1) has N eigenfuncions $\varphi_{\lambda_i} \in C^1(X)$ (with distinct λ_i) with $\mathrm{Re}\{\lambda_i\} < 0\alpha\nu\delta\nabla\varphi_{\lambda_i}(\boldsymbol{x}^*) \neq 0$. In addition, the eigenvalues λ_i are the eigenvalues of ϑ.

Proof. See [25], Proposition 2.

Corollary 1. Let $X \in \mathbb{R}^{\mathrm{N}}$ be a connected, forward invariant, compact set. Consider (1) with $f \in C^2(X)$ admits a hyperbolic fixed point $\boldsymbol{x}^* \in X$. If there exist N Koopman eigenfuncions $\varphi_{\lambda_i} \in C^1(X)$ with $\mathrm{Re}\{\lambda_i\} < 0$ and N vectors $\nabla\varphi_{\lambda_i}(\boldsymbol{x}^*) \neq 0$ are linearly independent. Then $\boldsymbol{x}^*$ is globally asymptotically stable.

Proof. See [25], Corollary 2.

Corollary 2. The Koopman eigenfunctions considered in Proposition 1 and Corollary 1 yield candidate Lyapunov functions as:

$$V(\boldsymbol{x}) = \left(\sum_{i=1}^{N} \|\varphi_{\lambda_i}(\boldsymbol{x})\|^2\right)^{1/2} \tag{14}$$

Proof. It is clear that $V(\boldsymbol{x}) > 0$ when $\xi \neq \boldsymbol{x}^*$ from the definition of the Koopman eigenfunction.

Apply the Koopman Operator to (14), we then have:

$$\begin{aligned}K^tV(\boldsymbol{x}) &= \left(\sum_{i=1}^{N} \|K^t\boldsymbol{\varphi}_{\lambda_i}(\boldsymbol{x})\|^2\right)^{1/2} \\ &= \left(\sum_{i=1}^{N} \|\mathrm{e}^{\lambda_i t}\boldsymbol{\varphi}_{\lambda_i}(\boldsymbol{x})\|^2\right)^{1/2} \\ &= \left(\sum_{i=1}^{N} \mathrm{e}^{2\,\mathrm{Re}\{\lambda_i\}t}\|\boldsymbol{\varphi}_{\lambda_i}(\boldsymbol{x})\|^2\right)^{1/2} < \mathrm{e}^{\mathrm{Re}\{\lambda_1\}t}V(\boldsymbol{x})\end{aligned} \tag{15}$$

where λ_1 is the eigenvalue closest to the complex axis and $\mathrm{P}\varepsilon\{\lambda_1\} < 0$. Then the time derivative of $\varsigma(\xi)$ is:

$$\begin{aligned}\dot{V}(\boldsymbol{x}) &= \lim_{t\to 0}\frac{K^t V(\boldsymbol{x}) - V(\boldsymbol{x})}{t} < \lim_{t\to 0}\frac{\mathrm{e}^{\mathrm{Re}\{\lambda_1\}t}-1}{t}V(\boldsymbol{x}) \\ &= \mathrm{Re}\{\lambda_1\}V(\boldsymbol{x}) < 0 \end{aligned} \tag{16}$$

This concludes the proof.

Proposition 1 provides a necessary and sufficient criterion for global stability, and Corollary 1 further extends to the asymptotical stability with more constraints on the eigenfunctions. The LF construction method is concluded in Corollary 2. The above theorems lay the foundation for stability analysis using the Koopman Operator. They can be regarded as a natural extension of the Hartman-Grobman theorem. More specifically, the local behavior of the dynamical system in the neighborhood of a hyperbolic equilibrium point is now extended to the whole feasible region.

III. Proposed Methodology

A. Region of Attraction Estimation

Once the LF is constructed, the ROA can be estimated directly from the LF. The main steps are summarized as follows:

1) Compute the time derivative of the LF

According to the chain rule:

$$\dot{V}(\boldsymbol{x}) = \left(\frac{\partial V}{\partial \boldsymbol{x}}\right)^{\mathrm{T}}\frac{\mathrm{d}\boldsymbol{x}}{\mathrm{d}t} = (\nabla V)^{\mathrm{T}} f(x) \tag{17}$$

From the chain rule, the first term of the time derivative is gradient of the LF, whereas the second term is the value of the ODE. Since the LF is numerically constructed, the first term of (17) can be easily estimated using the differential method.

2) Extract the region $\overline{X}$ where the LF is strictly decreasing

$$\overline{X} = \{\boldsymbol{x} \in X | \dot{V}(\boldsymbol{x}) < 0\} \cup \{\boldsymbol{x}^*\} \tag{18}$$

3) Estimate the ROA

Consider the largest level set $\partial B = \{\boldsymbol{x} \in \mathbb{R}^N | V(\boldsymbol{x}) \leq B\}$ such that $\partial B \subseteq \bar{X}$. ∂B is an inner approximation of the ROA.

B. EDMD Basis Function Construction for Swing Equation

The optimal construction of the EDMD basis function likely depends on the underlying dynamical system [18]. Possible choices include polynomials, radial basis functions (RBF), etc. However, the existing choices are not well suitable for power system models since the nonlinear functions often have the form of trigonometric functions, such as $\sin x$, $\cos x$. The classic post fault model for power system is described as:

$$\begin{aligned}&\begin{cases}\dot{\delta}_i = \omega_s \omega_i \\ \dot{\omega}_i = \frac{1}{M_i}(P_{mi} - P_{ei}(\delta)) - \frac{D_i}{M_i}\omega_i\end{cases} \\ &P_{ei}(\delta) = E_i^2 G_{ii} + \sum_{j,j\neq i} E_i E_j \left[B_{ij}\sin(\delta_i - \delta_j)\right. \\ &\qquad\qquad \left. + G_{ij}\cos(\delta_i - \delta_j)\right]\end{aligned} \tag{19}$$

where ω_s denotes the system angular frequency, δ_i and ω_i are the power angle and angular speed of generator i. M_i and D_i represent the generator inertia constants and damping coefficients, respectively. $P_{\mathrm{m}i}$ is the mechanical power input, and $P_{ei}(\delta)$ represents the electrical power output. E_i represents the voltage of bus i, and B_{ij} and G_{ij} are the line admittances and conductances. The polynomial basis function is the most widely used basis functions for EDMD. $Poly$-Q denotes the case where all monomials of the state variables up to degree Q. For example, *Poly*-3 of (19) is:

$$\Psi = [\delta, \omega, \delta^2, \delta\omega, \omega^2, \delta^3, \delta^2\omega, \delta\omega^2, \omega^3] \tag{20}$$

However, for the original polynomial basis function, it is difficult to express the nonlinearity of the trigonometric functions. It is proved that any nonlinear ODE can be rewritten in an exact equivalent quadratic-linear one [32], [33]. The transformation is done by the Lie derivatives. Using the SMIB system model as an example:

$$\begin{cases}\dot{\delta} = \omega_s \omega \\ \dot{\omega} = \frac{1}{M}(P_{\mathrm{m}} - P_{\mathrm{e}}\sin\delta - D\omega)\end{cases} \tag{21}$$

Let the coordinate transformation be:

$$x_1 = \delta,\ x_2 = \omega,\ x_3 = \sin\delta,\ x_4 = \cos\delta \tag{22}$$

Then (21) can be rewritten as:

$$\begin{cases}\dot{x}_1 = x_2 \\ \dot{x}_2 = \frac{1}{M}(P_{\mathrm{m}} - P_{\mathrm{e}}x_3 - Dx_2) \\ \dot{x}_3 = x_2 x_4 \\ \dot{x}_4 = -x_2 x_3\end{cases} \tag{23}$$

Now we can use the polynomial basis for (23), which implicitly contains trigonometric functions. We use *PolyT*-Q to denote the case considering the nonlinear function form of the swing equation, and *PolyT*-2 is shown as:

$$\begin{aligned}\Psi &= [x_1, x_2, x_3, x_4, x_2^2, x_2x_3, x_2x_4, x_3^2, x_4^2] \\ &= [\delta, \omega, \sin\delta, \cos\delta, \omega^2, \omega\sin\delta, \omega\cos\delta, \sin^2\delta, \cos^2\delta]\end{aligned} \tag{24}$$

C. EDMD Basis Function Construction for PLL Dynamics

Consider the system of VSC connected to the AC grid [34], as shown in Fig. 1. The AC grid is modeled by an ideal voltage source U_{g} in series with the grid impedance Z_{g}. The connection strength is reflected by the value of the grid impedance. The VSC is synchronized to the AC grid by the phase lock loop (PLL), which adjusts angular speed and provides a synchronizing phase by detecting terminal voltage

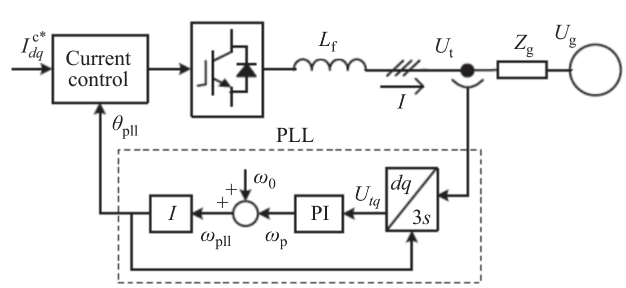

Fig. 1. The system of VSC connected to a weak AC grid.

at the point of common coupling (PCC), denoted as U_{t}. If the AC grid is weak and the grid impedance is large, the PLL dynamics of synchronizing control is significantly influenced by the PCC voltage. The governing equation of the VSC PLL during severe grid fault is derived in [34] and shown in (25).

$$\begin{cases} \dot{\delta} = \omega \\ \dot{\omega} = \frac{k_{\mathrm{i}}}{1-\frac{k_{\mathrm{p}} X_{\mathrm{g}} i_d^{\mathrm{c}*}}{\omega_s}} \Big[X_{\mathrm{g}} i_d^{\mathrm{c}*} + R_{\mathrm{g}} i_q^{\mathrm{c}*} - U_{\mathrm{g}} \sin\delta \\ \qquad - \left(\frac{k_{\mathrm{p}}}{k_{\mathrm{i}}} U_{\mathrm{g}} \cos\delta - \frac{X_{\mathrm{g}} i_d^{\mathrm{c}*}}{\omega_s} \right) \omega \Big] \end{cases} \tag{25}$$

where ω denotes the PLL's angular speed in the PLL reference frame and δ is the integration of ω, which is called the virtual power angle in some literature. k_{i} and k_{p} are the PLL's integral and proportional coefficients, respectively. X_{g} and R_{g} represent the grid impedance. $i_d^{\mathrm{c}*}$ and $i_q^{\mathrm{c}*}$ are the d-axis and q-axis components of the current reference. Comparing (21) and (25), it can be concluded that the PLL dynamics is close to the swing equation of the SMIB system [35]. The difference lies in that the damping effect of the SMIB system can be regarded as a constant coefficient, while that of the PLL dynamics is a function of the virtual power angle. This difference makes the PLL dynamics more complicated to analyze. Nevertheless, we can still use (22) to convert the PLL dynamics (25) to a quadratic-linear ODE. In other words, the polynomial basis function *PolyT*-Q is valid to approximate the ROA for both SMIB and VSC PLL systems. We present the approximation result side by side to compare the commons and differences of the two systems in Section IV.

D. Algorithm Summary

This subsection summarizes the proposed methodology in a step-by-step manner.

Step 1: Randomly choose initial conditions from the state space, compute the trajectories using numerical integration, and evenly sample from the trajectories to generate a dataset of state variable snapshot pairs $\boldsymbol{X}$ and $\boldsymbol{Y}$ as in (8).

Step 2: Create a set of basis functions using the method proposed in Section III-B, and lift the system dynamics to generate $\boldsymbol{X}_{\mathrm{lift}}$ and $\boldsymbol{Y}_{\mathrm{lift}}$ as in (10).

Step 3: Compute the finite-approximation of the Koopman Operator K with (11), and compute the spectral decomposition of the operator with (12).

Step 4: Construct the candidate LF with the Koopman eigenfunctions using (14), and compute the time derivatives of the LF using (17).

Step 5: Extract the region where LF is strictly decreasing as in (18), and estimate the ROA by the largest level set in the region.

As a result of the procedure above, we have a set of Koopman eigenvalues and eigenfunctions to track the nonlinear dynamics of the system. We also have the LF to capture the geometric properties of the ROA. Ultimately, the proposed method is a data driven procedure that can be applied to systems without a precise model as long as we can monitor the state trajectories.

IV. Case Studies and Discussions

In this section, an illustrative example with the finite dimension Koopman Operator is first presented to show the basic logic of the proposed method. Then the ROA of the SMIB and the VSC PLL system is approximated by the proposed method. The geometric properties discovering function is demonstrated by the TMIB system taken from [12]. In addition, we will compare the proposed method with the state-of-the-art numerical LF construction method SOS developed in [12], [13].

A. An Illustrative Example

Consider the so called fast-slow manifold system (26) with a global asymptotically stable equilibrium point at (0, 0) if and only if $\mu < 0, \eta < 0$.

$$\begin{cases} \dot{x}_1 = \mu x_2 \\ \dot{x}_2 = \eta (x_2 - x_1^2) \end{cases} \tag{26}$$

The eigenvalues of the Jacobian matrix at the SEP are μ and η. It is easy to verify that the corresponding eigenfunctions are:

$$\begin{aligned} \varphi_\mu &= x_1 \\ \varphi_\eta &= x_2 - b x_1^2,\ b = \frac{\eta}{\eta - 2\mu} \end{aligned} \tag{27}$$

Then the LF is $V = \sqrt{\varphi_\mu^2 + \varphi_\eta^2}$ and the derivative to time is:

$$\dot{V} = \frac{\partial V}{\partial x_1}\dot{x}_1 + \frac{\partial V}{\partial x_2}\dot{x}_2 = \frac{\mu x_1^2 + \eta\left(x_2 - b x_1^2\right)^2}{\sqrt{x_1^2 + \left(x_2 - b x_1^2\right)^2}} \tag{28}$$

If $\mu < 0, \eta < 0$, we have $\dot{V} < 0$ for any $x_1, x_2 \in \mathbb{R}$. Therefore, we can verify the global asymptotically stable necessary and sufficient criterion of (26) with the proposed method.

B. The ROA of the SMIB and VSC PLL System

Consider the SMIB system (21), and the parameters that are given in the Appendix. There is no analytic Koopman Operator for (21) or (25), so we numerically approximate the operator and ROA. We perform numerical integration of two system ODEs with a fixed time step of 0.01 s for 1,000 randomly chosen initial points, each trajectory contains 10 snapshots. We use *PolyT*-5 as the basis function.

The surface plot and the contour plot of the LF is shown in Fig. 2. The SMIB system has one SEP at (0.82, 0) and one UEP at (2.32, 0), which is a saddle node. Similarly, the VSC PLL system also has one SEP at (0.78, 0) and one saddle node at (2.37, 0). From the left plots of Fig. 2, it is clear that the approximated LF recovers the properties of the two Eps. The SEP is located at the bottom of the ROA, while the saddle node is at the boundary.

The black dashed line in the right plots shows the theoretical ROA and the magenta line represents the estimated one using the proposed method. We can estimate that the UEP of the SMIB and the VSC PLL system is around (2.31, −0.07) and (2.36, −0.22), respectively. Therefore, the estimated UEPs and ROA are quite close to the ground truth. In addition, it can be observed that the shapes of the contour lines of the

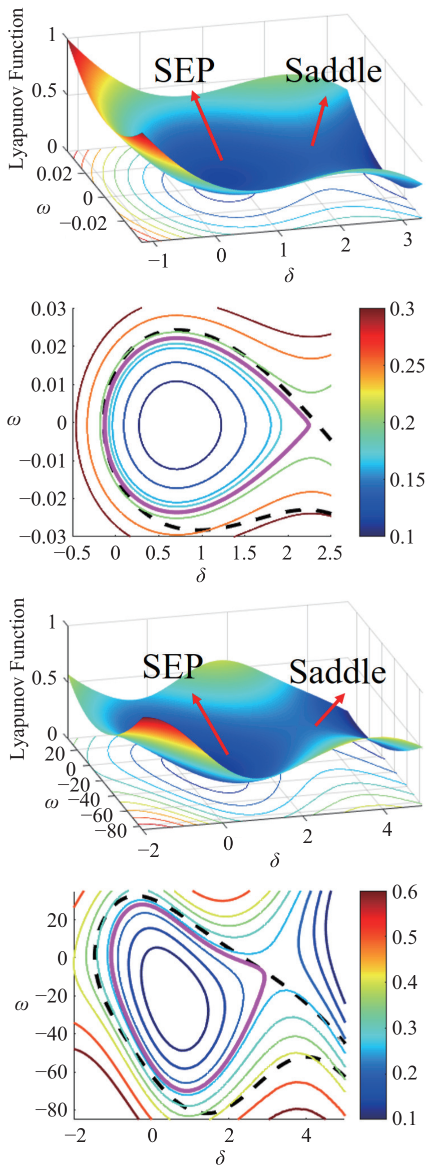

Fig. 2. Lyapunov function of the SMIB and VSC PLL system. Top row: surface plot and contour plot of the SMIB system; bottom row: surface plot and contour plot of the VSC PLL system.

numerical LF aligns with the theoretical ROA shape. Thus, the approximated LF can retain the geometric properties of the system. This unique characteristic will be further proven in a multiple UEPs test case below. Compare the top right and bottom right plots; it is found that that both real and approximated ROA of the VSC PLL system have a steeper slop than the SMIB system. This is because the damping coefficient is affected by the virtual power angle of the VSC PLL system. In some value ranges, it can even become negative in order to make the ROA smaller.

In addition, the critical clearing time (CCT) can also be estimated using the values of the LF along the time during a fault on status, as shown in Fig. 3. The largest LF level set that satisfies (18) is around 0.232. From the fault-on trajectory of the LF values, it can be seen that the approximated CCT is 0.11 s. And the real CCT is about 0.14 s as determined from simulations. The right plot of Fig. 3 shows the phase portrait of a stable case (blue line, clearing time 0.10 s) and an unstable case (red line, clearing time 0.15 s). The intersection between the fault-on phase portrait and the ROA is quite close for the SEP (denoted by the red star).

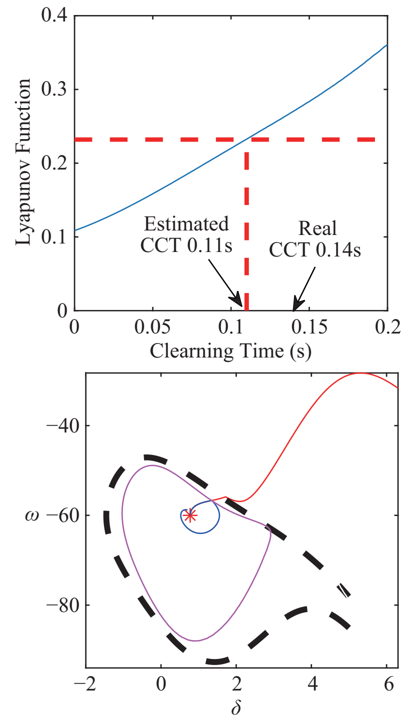

Fig. 3. Finding the CCTs using the Lyapunov function. Left: Lyapunov function value along time during fault; right: Phase portrait of a stable case and an unstable case.

C. The Geometric Properties of the TMIB System

The TMIB system is taken from [12] and [36], which has been discussed extensively as a power system model with conductances that does not have analytical energy functions by the traditional direct method. The system model is shown in (29) after shifting the fixed point to (0, 0, 0, 0). x_1 and x_3 represent the power angle of machine 1 and 2, whereas x_2 and x_4 denote the angular speed, respectively.

$$\begin{cases} \dot{x}_1 = x_2 \\ \dot{x}_2 = 16.9715\cos x_1 \sin x_3 - 31.6131\cos x_1 \\ \qquad -50.8269\sin x_1 - 1.9718\cos x_1\cos x_3 \\ \qquad -16.9715\cos x_3 \sin x_1 - 1.8868 x_2 \\ \qquad -1.9718\sin x_1 \sin x_3 + 33.5849 \\ \dot{x}_3 = x_4 \\ \dot{x}_4 = 11.3986\cos x_3 \sin x_1 - 47.2723\cos x_3 \\ \qquad -87.4618\sin x_3 - 1.2088\cos x_1 \cos x_3 \\ \qquad -11.3986\cos x_1 \sin x_3 - 1.2658 x_4 \\ \qquad -1.2088\sin x_1 \sin x_3 + 48.4810 \end{cases} \tag{29}$$

Similar to the experiment settings of [12], we exam the ROA projected in the angle space when $\omega_1 = \omega_2 = 0.8$ p.u. The surface plot of the LF constructed from the proposed method and the SOS method is shown in Fig. 4. The LF equation from the SOS method can be found in Section VII-D in [12]. The

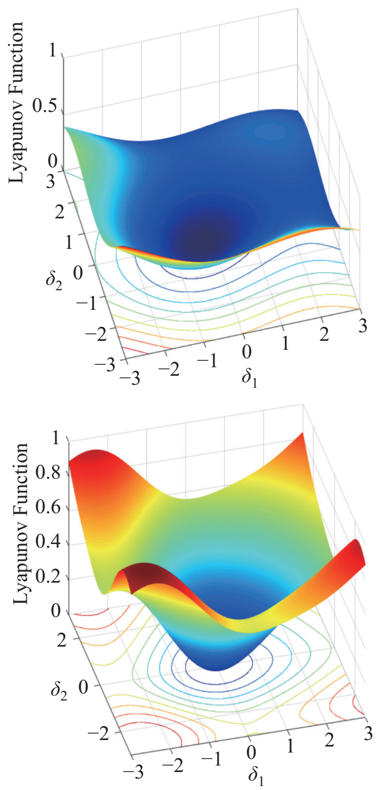

Fig. 4. Lyapunov function of the TMIB system. Left: LF constructed using the proposed method, right: LF constructed using SOS [12].

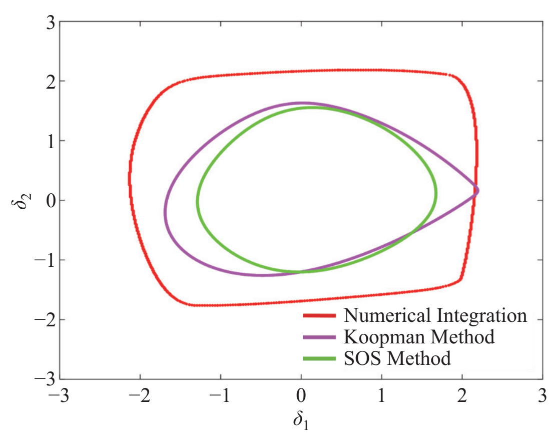

Fig. 5. Estimated ROA with different methods.

red line in Fig. 5 is the theoretical ROA computed by extensive numerical simulations. The magenta line denotes the estimated ROA using the proposed method while the green line is from the SOS method in [12]. It is clear that the proposed method causes a less conservative estimation than the SOS method.

More importantly, we argue that the Koopman eigenfunction is capable of capturing the geometric properties that the SOS method fails to track. The level sets of the LF in shown in Fig. 6. The black arrows denote the trajectory directions at each point of the power angle state space. We can observe that there is one SEP located at origin (point A), two saddle nodes (point B and C) and one unstable node (point D) located on the boundary. The equilibrium types can be verified by the

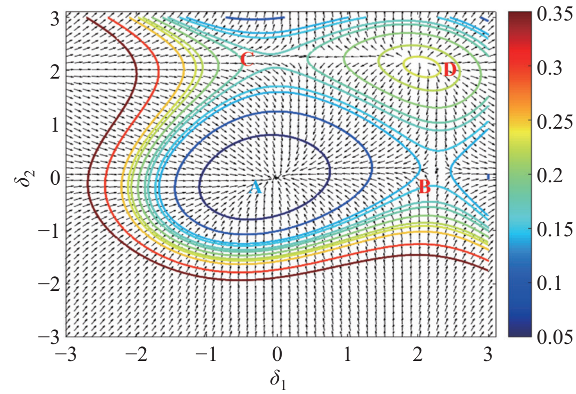

Fig. 6. Level sets of the Lyapunov function of the TMIB system.

trajectory directions. The discovery of the UEPs around the SEP can provide significant information about potential instability modes. This is another key advantage of the Koopman Operator based stability analysis.

D. Discussions and Future Study

We have introduced a Koopman Operator based algorithm for the consturction of LF and the estimation of ROA. The method has two unique features to distinguish it from traditional transient stability analysis methods.

One is that the method is data driven and capable of providing a systematic approach for computing the LF for any power system models. For example, Section IV-C shows that the proposed method is valid for systems with transfer conductances, whose analytical energy functions do not exist, or exist with certain assumptions according to [35]. Moreover, the power electronics dominated power systems have introduced lots of new nonlinear functions into the power system models, so that it is even harder for traditional direct methods to find proper energy functions. In contrast, the proposed method can be generalized to numerically construct the LF and estimate the ROA of such systems, thus providing alternative approaches to analyzing the stability of the new power electronics dominated power systems.

The other unique feature is the ability to capture the geometric properties of the manifold, which is vital to understanding the characteristics of the equilibrium points and provide useful information to the instability modes.

Nevertheless, before the proposed method can be applied to large power systems, there are certain barriers. The difficulties are not conceptual but numerical because there would always be some truncation errors when trying to approximate the infinite dimensional Koopman Operator using a finite dimensional matrix, even though we have reduced the errors using the proposed new basis functions. For example, the location of the saddle node C discovered by the algorithm is a bit different from the results concluded from the arrows of the vector field. It is preferred to design some theoretical convergent series (e.g., the Laurent series [31] or other orthogonal polynomial series) as a basis function so that the truncation error can be controlled and analytically estimated. Other researchers are trying to use deep neural networks to construct the implicit basis functions [37], [38] and have already made some progress.

Secondly, the data used to approximate the Koopman Operator are the state variables, which are gathered from numerical integration. So we still need the model information at the current stage. The adaptability when the model changes can be improved in two ways. One is to develop an online algorithm to update the Koopman Operator in a real-time manner so that the Koopman Operator can be more accurate as more data accumulates. The other one is to develop methods using the responses from random perturbation to approximate the Koopman Operator [39]. In such cases, the measured data from PMUs are expected to provide the same information so that a 100% free model can be achieved.

The third issue needing attention is how to numerically compute the level sets in high-dimensional spaces. Currently we can only approximate the level sets in 2D space so that we project the ROA of the TMIB system to the $\delta_1 - \delta_2$ plane. Future breakthroughs on this point will enable us to simultaneously analyze more than two parameters.

V. Conclusion

This paper proposes a Koopman Operator based method to numerically construct the Lyapunov functions and estimate the region of attraction for power system transient stability analysis. The spectral decomposition of the operator contains key stability information, including the geometric properties of the manifold.

The ultimate goal is to build a data driven framework to only use measurements to analyze the stability of a nonlinear system, with unknown or imprecise governing equations. In order to achieve the ultimate goal, the Koopman Operator approximation algorithm needs to be improved. We have provided potential research directions in Section IV-D. In addition, efforts should be made to investigate how the input data which is related to the operator approximation. For example, whether partial measurements will increase the approximation errors.

Appendix

The parameters of the SMIB system and the VSC PLL system is in Appendix Tables AI and AII.

TABLE AI
Parameters of the SMIB System

Symbols	Descriptions	Values
ω_s	angular frequency	100π rad·s^{-1}
M	inertia constant	6 rad·s^2
D	damping coefficient	5 rad·s
P_m	mechanical power input	1.20 p.u.
P_e	maximum electrical power	1.64 p.u.

TABLE AII
Parameters of the VSC PLL System

Symbols	Descriptions	Values
$k_\mathrm{p}, k_\mathrm{i}$	PI parameters of PLL	50, 1300
$i_d^{\mathrm{c}*}, i_q^*$	D-axis and q-axis current reference during grid fault	-0.6 p.u., 0.4 p.u.
$L_\mathrm{g}, R_\mathrm{g}$	grid impedance	0.5 p.u., 0.05 p.u.
U_g	residual grid voltage during grid fault	0.4 p.u.

Acknowledgment

We would like to thank Alexandre Mauroy and Masih Haseli for many fruitful discussions in preparation of this paper.

References

[1] P. Kundur, J. Paserba, V. Ajjarapu, G. Andersson, A. Bose, C. Canizares, N. Hatziargyriou, D. Hill, A. Stankovic, C. Taylor, T. Van Cursem, and V. Vittal, "Definition and classification of power system stability," *IEEE Transactions on Power Systems*, vol. 19, no. 3, pp. 1387–1401, Aug. 2004.

[2] N. Hatziargyriou, J. Milanović, C. Rahmann, V. Ajjarapu, C. Cañizares, I. Erlich, D. Hill, I. Hiskens, I. Kamwa, B. Pal, P. Pourbeik, J. Sanchez-Gasca, A. Stanković, T. Van Cutsem, V. Vittal, and C. Vournas, "Stability definitions and characterization of dynamic behavior in systems with high penetration of power electronic interfaced technologies," IEEE Power and Energy Society, Piscataway, NJ, USA, Tech. Rep. PES-TR77, Apr. 2020.

[3] P. Kundur, *Power System Stability and Control*. New York: McGraw-Hill, 1994.

[4] Y. S. Xue, "A critical comparison of various methods for transient stability assessment part one disturbed-measure functions," *Automation of Electric Power Systems*, vol. 25, no. 11, pp. 6–11, Jun. 2001.

[5] L. Zheng, W. Hu, Y. F. Zhou, Y. Min, X. L. Xu, C. M. Wang, and R. Yu, "Deep belief network based nonlinear representation learning for transient stability assessment," in *2017 IEEE Power & Energy Society General Meeting*, 2017, pp. 16–20.

[6] S. Wu, L. Zheng, W. Hu, R. Yu, and B. S. Liu, "Improved deep belief network and model interpretation method for power system transient stability assessment," *Journal of Modern Power Systems and Clean Energy*, vol. 8, no. 1, pp. 27–37, Jan. 2020.

[7] W. L. Zhang, W. Hu, Y. Min, L. Chen, and X. Z. Liu, "Conservative online transient stability assessment in power system based on concept of stability region," *Power System Technology*, vol. 40, no. 4, pp. 992–998, Apr. 2016.

[8] W. S. Cheng, L. Zheng, and J. Wu, "Conditional mutual information based interpretable key feature selection method for power system security analysis," presented at the *5th Conference on Energy Internet and Energy System Integration*, Taiyuan, China, 2021, pp. 22–24.

[9] H. D. Chiang, *Direct Methods for Stability Analysis of Electric Power Systems: Theoretical Foundation, BCU Methodologies, and Applications*. Hoboken, NJ: Wiley, 2011.

[10] Y. Zou, M. H. Yin, and H. D. Chiang, "Theoretical foundation of the controlling UEP method for direct transient-stability analysis of network-preserving power system models," *IEEE Transactions on Circuits and Systems I: Fundamental Theory and Applications*, vol. 50, no. 10, pp. 1324–1336, Oct. 2003.

[11] H. D. Chiang, J. Z. Tong, and Y. Tada, "On-line transient stability screening of 14,000-bus models using TEPCO-BCU: Evaluations and methods", in *Proceedings of the IEEE PES General Meeting*, 2010, pp. 1–8.

[12] M. Anghel, F. Milano, and A. Papachristodoulou, "Algorithmic construction of Lyapunov functions for power system stability analysis," *IEEE Transactions on Circuits and Systems I: Regular Papers*, vol. 60, no. 9, pp. 2533–2546, Sep. 2013.

[13] H. Choi, P. J. Seiler, and S. V. Dhople, "Robust power systems stability assessment with sum of squares optimization," in *Proceedings of the 2015 IEEE Power & Energy Society General Meeting*, 2015, pp. 1–5.

[14] I. Mezić, "Spectral properties of dynamical systems, model reduction and decompositions," *Nonlinear Dynamics*, vol. 41, no. 1–3, pp. 309–325, Aug. 2005.

[15] H. Arbabi and I. Mezić, "Ergodic theory, dynamic mode decomposition, and computation of spectral properties of the Koopman operator," *SIAM Journal on Applied Dynamical Systems*, vol. 16, no. 4, 2096–2126, Nov. 2017.

[16] A. Mauroy, I. Mezić, and Y. Susuki, *The Koopman Operator in Systems and Control: Concepts, Methodologies, and Applications*. Cham: Springer International Publishing, 2020.

[17] J. H. Tu, C. W. Rowley, D. M. Luchtenburg, S. L. Brunton, and J. N. Kutz, "On dynamic mode decomposition: Theory and applications," *Journal of Computational Dynamics*, vol. 1, no. 2, pp. 391–421, May 2014.

[18] M. O. Williams, I. G. Kevrekidis, and C. W. Rowley, "A data-driven approximation of the Koopman operator: Extending dynamic mode decomposition," *Journal of Nonlinear Science*, vol. 25, no. 6, pp. 1307–1346, Jun. 2015.

[19] M. Haseli and J. Cortés, "Learning Koopman Eigenfunctions and invariant subspaces from data: Symmetric subspace decomposition," *IEEE Transactions on Automatic Control*, vol. 67, no. 7, pp. 3442–3457, Jul. 2022.

[20] M. Haseli and J. Cortés, "Data-driven approximation of Koopman-invariant subspaces with tunable accuracy," in *Proceedings of the 2021 American Control Conference (ACC)*, 2021, pp. 1–6.

[21] M. Korda and I. Mezić, "Linear predictors for nonlinear dynamical systems: Koopman operator meets model predictive control," *Automatica*, vol. 93, pp. 149–160, Jul. 2018.

[22] E. Kaiser, J. N. Kutz, and S. L. Brunton, "Data-driven discovery of Koopman eigenfunctions for control," *Machine Learning: Science and Technology*, vol. 2, no. 3, pp. 035023, Jun. 2021.

[23] A. Mauroy and J. Goncalves, "Koopman-based lifting techniques for nonlinear systems identification," *IEEE Transactions on Automatic Control*, vol. 65, no. 6, pp. 2550–2565, Jun. 2020.

[24] A. Mauroy, I. Mezić, and J. Moehlis, "Isostables, isochrons, and Koopman spectrum for the action-angle representation of stable fixed point dynamics," *Physica D: Nonlinear Phenomena*, vol. 261, pp. 19–30, Oct. 2013.

[25] A. Mauroy and I. Mezić, "Global stability analysis using the eigenfunctions of the Koopman operator," *IEEE Transactions on Automatic Control*, vol. 61, no. 11, pp. 3356–3369, Nov. 2016.

[26] Y. Susuki and I. Mezic, "Nonlinear Koopman modes and a precursor to power system swing instabilities," *IEEE Transactions on Power Systems*, vol. 27, no. 3, pp. 1182–1191, Aug. 2012.

[27] Y. Susuki and I. Mezić, "Nonlinear Koopman modes and power system stability assessment without models," *IEEE Transactions on Power Systems*, vol. 29, no. 2, pp. 899–907, Mar. 2014.

[28] E. Barocio, B. C. Pal, N. F. Thornhill, and A. R. Messina, "A dynamic mode decomposition framework for global power system oscillation analysis," *IEEE Transactions on Power Systems*, vol. 30, no. 6, pp. 2902–2912, Nov. 2015.

[29] M. A. Hernández-Ortega and A. R. Messina, "Nonlinear power system analysis using Koopman mode decomposition and perturbation theory," *IEEE Transactions on Power Systems*, vol. 33, no. 5, pp. 5124–5134, Sep. 2018.

[30] H. Choi and S. Bose. Transient stability analysis of power systems using Koopman Operators [Online]. Available: http://boses.ece.illinois.edu/files/TSKoopman.pdf, 2018.

[31] S. L. Brunton, M. Budišić, E. Kaiser, and J. N. Kutz, "Modern Koopman theory for dynamical systems," *SIAM Review*, vol. 64, no. 2, pp. 229–340, May 2022.

[32] C. J. Gu, "QLMOR: A projection-based nonlinear model order reduction approach using quadratic-linear representation of nonlinear systems," *IEEE Transactions on Computer-Aided Design of Integrated Circuits and Systems*, vol. 30, no. 9, pp. 1307–1320, Sep. 2011.

[33] M. Netto, Y. Susuki, V. Krishnan, and Y. C. Zhang, "On analytical construction of observable functions in extended dynamic mode decomposition for nonlinear estimation and prediction," *IEEE Control Systems Letters*, vol. 5, no. 6, pp. 1868–1873, Dec. 2021.

[34] Q. Hu, L. J. Fu, F. Ma, and F. Ji, "Large signal synchronizing instability of PLL-based VSC connected to weak AC grid," *IEEE Transactions on Power Systems*, vol. 34, no. 4, pp. 3220–3229, Jul. 2019.

[35] Y. Liu, M. Huang, X. Zha and H. H. -C. Iu, "Transient current estimation of MMC-HVDC systems under a grid-converter phase difference," *CSEE Journal of Power and Energy Systems*, vol. 7, no. 4, pp. 730–743, Jul. 2021.

[36] N. G. Bretas and L. F. C. Alberto, "Lyapunov function for power systems with transfer conductances: Extension of the invariance principle," *IEEE Transactions on Power Systems*, vol. 18, no. 2, pp. 769–777, May 2003.

[37] Q. X. Li, F. Dietrich, E. M. Bollt, and I. G. Kevrekidis, "Extended dynamic mode decomposition with dictionary learning: A data-driven adaptive spectral decomposition of the Koopman operator," *Chaos*, vol. 27, no. 10, pp. 103111, Oct. 2017.

[38] B. Lusch, J. N. Kutz, and S. L. Brunton, "Deep learning for universal linear embeddings of nonlinear dynamics," *Nature Communications*, vol. 9, no. 1, pp. 4950, Nov. 2018.

[39] X. Li, C. Mishra, S. Chen, Y. Wang and J. De La Ree, "Determination of parameters of time-delayed embedding algorithm using Koopman operator-based model predictive frequency control," *CSEE Journal of Power and Energy Systems*, vol. 7, no. 6, pp. 1140–1151, Nov. 2021.

Le Zheng (M'12) received the B.S. and Ph.D. degrees in Electrical Engineering from Tsinghua University, Beijing, China, in 2011 and 2017, respectively. He had been a Postdoctoral Research Fellow in Stanford University from 2017 to 2019. He is currently a faculty member of the North China Electric Power University, Beijing, China. His current research interests include stability and control of power electronics dominated power systems and renewable energy conversion systems, and machine learning applications in power systems.

Xin Liu received the B.S. degrees in Electrical Engineering from Northeast Electric Power University, JiLin, China, in 2021. He is currently pursuing the master's degrees with the North China Electric Power University, Beijing, China. His current research interests include stability and control of power electronics dominated power systems and renewable energy conversion systems.

Yanhui Xu (M'07) received the B.S., M.S., and Ph.D. degrees from North China Electric Power University, Beijing, China, in 2001, 2004, and 2010, respectively. He is currently a Full Professor with the School of Electrical and Electronic Engineering, North China Electric Power University. His research interests include power system subsynchronous oscillation, low-frequency oscillation, and load modeling.

Wei Hu received the B.S. and Ph.D. degrees in Electrical Engineering from Tsinghua University, China, in 1998 and 2002, respectively and is now a Researcher there. His research interests include power system analysis and control, Big Data technology in power system, multi-type power generator-grid coordination and control, optimization control between renewable energy and energy storage system.

Chongru Liu (M'10–SM'15) received her B.S., M.S. and Ph.D. degrees in Electrical Engineering from Tsinghua University, Beijing, China. She was a visiting professor at the University of Hong Kong from 2009 to 2010, and she was a visiting professor at Washington State University from 2010 to 2011. She is currently a professor in the School of Electrical and Electronic Engineering, North China Electric Power University. She is a member of the National Power System Management and Information Exchange Standardization Committee of China. She is a member of Beijing Nova and supported by the program of New Century Excellent Talents in University. Her research interests include analysis, simulation and control of AC / DC hybrid system.